Available online at www.sciencedirect.com

SciVerse ScienceDirect

Ceramics International 39 (2013) 209–218

CERAMICS INTERNATIONAL

www.elsevier.com/locate/ceramint

A novel foam-like silane modified alumina scaffold coated with nano-hydroxyapatite–poly(ε-caprolactone fumarate) composite layer

Sedigheh Joughehdoust[a,*], Aliasghar Behnamghader[b], Mohammad Imani[c], Morteza Daliri[d], Azadehsadat Hashemi Doulabi[e], Ebrahim Jabbari[b]

[a]*Department of Biomedical Engineering, Science and Research Branch, Islamic Azad University, Tehran, Iran*
[b]*Biomaterials group, Materials & Energy Research Center, Tehran, Islamic Republic of Iran, Postal code 13145-1659*
[c]*Novel Drug Delivery Systems Dept., Iran Polymer and Petrochemical Institute, P.O. Box 14965/115, Tehran, Iran*
[d]*National Institute for Biotechnology and Genetic Engineering, Tehran, Iran*
[e]*Polymer Engineering Department, Amirkabir University of Technology, P.O. Box 15875/4413, Tehran, Iran*

Received 18 April 2012; received in revised form 2 June 2012; accepted 4 June 2012
Available online 15 June 2012

Abstract

Although alumina scaffolds with biodegradable polymer coating can overcome the limitations of conventional ceramic bone substitutes, the bioactivity potential of these scaffolds needs to be enhanced. In this study, the macroporous alumina scaffolds with the defined pore-channel interconnectivity were successfully prepared by the foam replication method. The average pore size of the scaffolds was in the range 200–900 μm with around 82% porosity. The average Young's modulus of alumina scaffolds was 2.8 GPa. Coating of nano-hydroxyapatite (nano-HA) in poly(ε-caprolactone fumarate) (PCLF) as a carrier on the surface of alumina scaffold was performed. The nano-HA powder was synthesized successfully by the sol–gel method. The crystallite and particle sizes of HA powders were in nano range and confirmed by the Scherrer equation from X-ray diffraction (XRD), scanning electron microscopy (SEM) and transmission electron microscopy (TEM). The PCLF was synthesized and characterized by fourier transform infrared spectroscopy (FTIR) and differential scanning calorimetry (DSC). In order to make a chemical link between the alumina scaffolds and the coating, a silane coupling agent was used. The results showed that using of 1 g Methacryloxypropyl trimethoxysilane in 100 g solvent is sufficient for making a thin interface layer between the scaffold and the polymer. The coating process was performed by immersion of scaffolds in the solutions with different percents of nano-HA. The morphology and chemical structure of the coated scaffolds were investigated by SEM and FTIR. SEM images demonstrated that the scaffolds were constituted of interconnected and homogeneously distributed pores. Also, HA distribution and agglomerates on the surface of scaffolds were enhanced by increasing the nano-HA percent in the coating solutions.

Keywords: B. Nanocomposites; Alumina scaffold; Poly(ε-caprolactone fumarate); Hydroxyapatite

1. Introduction

Over the last decade, porous bioceramics with open pore structures have obtained a great deal of attention for treating of damaged bones, since they let bone cells go through the interconnected pores and grow on their biocompatible surfaces [1–4]. Highly open interconnected porous bioceramic scaffolds provide a three-dimensional environment for growing the new tissue, where cell culture medium and growth factors can be easily accessible through the open pores. One of the most important requirements for making a suitable scaffold for bone tissue engineering is the formation of an appropriate scaffold to bear the mechanical stress and align the growth of new bone [5,6]. They are bioinert ceramics (e.g., alumina and zirconia), bioactive ceramics (e.g., bioglasses and hydroxyapatite) and biodegradable ceramics (e.g., tri-calcium phosphate and bone cement).

The scaffolds for bone regeneration should mimic the structure and properties of the bone extra-cellular matrices. Since bone consists of a porous composite of

*Corresponding author.
E-mail address: joughehdoust@gmail.com (S. Joughehdoust).

0272-8842/$36.00
http://dx.doi.org/10.1016/j.ceramint.2012.06.011

interpenetrating phases of hydroxyapatite and collagen, the scaffolds for bone regeneration should be similarly porous composites with interpenetrating ceramic and polymer phases. The problem of hydroxyapatite and other calcium phosphate is their poor mechanical properties such as low strength and high brittleness. Alumina is a suitable material for this application as it possesses an acceptable biocompatibility besides the mechanical properties better than calcium phosphates [7].

Polymer phases can fill the cracks of bioceramic and thus the mechanical properties of brittle ceramic scaffolds would be improved by coating of polymer layers. It is hypothesized that polymer filaments may bridge cracks during fracture thus increasing the scaffold toughness, in a similar manner as collagen fibers enhancing the fracture toughness of bone [8].

Fumarate based unsaturated polyesters including poly (propylene fumarate) [9,10], poly(ethylene glycol fumarate) (PPF) [11], poly(caprolactone fumarate) (PCLF) [12–14] and recently poly(hexamethylene carbonate fumarate) [15] have been developed because of their inherent biocompatibility and ease of process ability. On the other hand, poly(caprolactone fumarate) as a novel biodegradable and biocompatible polymeric system was selected for the polymer coating phase on alumina scaffolds. However, they generally lack sufficient cell attachment and osteoconductive properties due to the usual surface properties of polymeric materials such as negligible surface energy [16]. In addition, the polymer phase can be a carrier for drugs and other biomolecules and bioactive agents hence enhancing the functionality and bioactivity of the scaffolds. Hydroxyapatite (HA) nanoparticles can be used in polymer coatings for optimizing cell attachment, bioactivity and osteoconductivity [17].

Organofunctional trialkoxysilanes are usually used to bind organic polymers to inorganic mineral surfaces such as alumina. The chemical structure of organofunctional trialkoxysilanes is $RSiX_3$ where R is an organofunctional group and X is a hydrolysable alkoxy group. Reaction of alkoxysilane coupling agents includes four distinct steps as shown in Fig. 1 [18] which clearly shows that hydroxyl (–OH) groups play a vital role in binding a monolayer of the alkoxysilane coupling agent to the surface of substrate.

The replication technique (or polymer sponge method) [19] produces porous ceramic structures that are similar to those of spongy bone [20,21]. This method includes preparation of green bodies of ceramic foams by coating polymer foam (e.g. polyurethane, PU) with ceramic slurry. The polymer has a desired pore structure with proper internal channel architecture which can be used as a template for producing ceramic scaffolds.

In the present paper, we studied the synthesis of nano-HA and poly(caprolactone fumarate), fabrication of alumina scaffold and coating of poly(caprolactone fumarate)/nano-HA composite layer on the scaffolds.

2. Materials and methods

2.1. Synthesis of nano-HA

In this research, nano-HA was synthesized by the sol–gel method. Triethyl phosphite [TEP, $(C_2H_5O)_3P$; Merck] and calcium nitrate tetrahydrate [$Ca(NO_3)_2 \cdot 4H_2O$; Merck] were used as P and Ca precursors, respectively. First, a solution of TEP in ethanol was prepared and in a separate container, calcium nitrate tetrahydrate was dissolved in ethanol. Both of the solutions were vigorously agitated for 24 h. Subsequently, the Ca containing solution was added to the P-containing, one dropwise (Ca/P = 1.67). The concentrations of both the solutions were 2 M. The resulting sol was kept at room temperature for 96 h. The gel was dried at 70 °C for 3 days and then heat-treated at 550 °C for 1 h. Phase composition of nano-HA powder was studied by XRD (D500, Siemens, Germany). Scanning electron microscope (SEM, XL30, Philips, Holland) and transmission electron microscope (TEM, CM200FEG, Philips) were used for observation of the powder morphology.

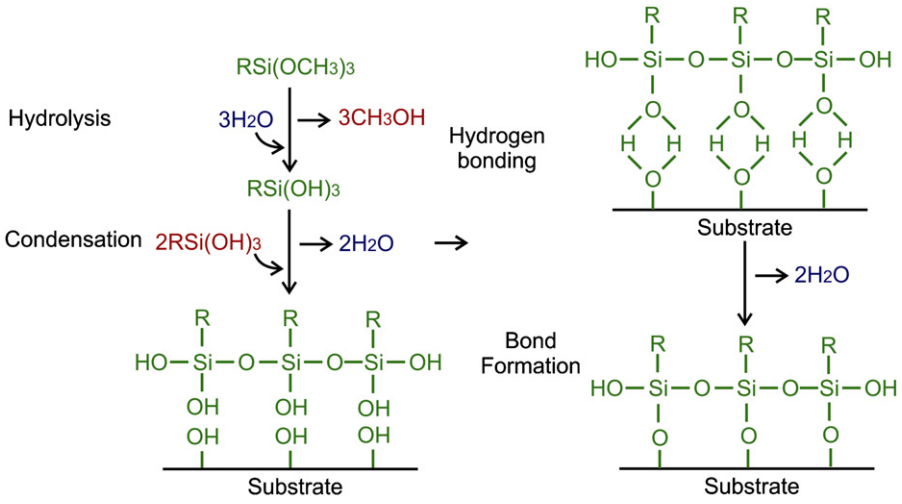

Fig. 1. Reaction scheme of trialkoxy silane reaction with a surface [18].

The size of the crystallites was estimated by the Scherrer equation [22]: where D is the size of the crystallite in Å, K is the shape factor of the average crystallite (approximately equals 0.9), λ is the X-ray wavelength, β is the line broadening at half the maximum intensity (FWHM) in radians, and θ is the Bragg angle:

$$D = \frac{K\lambda}{\beta \cos\theta} \quad (1)$$

2.2. Synthesis of PCLF

The PCLF samples were synthesized using poly(ε-caprolactone diol) (PCL-diol) with a number average molecular weight (M_n) of 530 g/mol, fumaryl chloride (FuCl), and propylene oxide (PO) were purchased from Aldrich Chemical Co. (Milwaukee, MN, USA). The purified FuCl, PCL-diols, and PO were reacted in 0.99:1:2 molar ratios, respectively. First, the PCL diol was dissolved in dichloromethane (DCM, Merck Co.) and PO was added to this solution. The FuCl was dissolved in DCM and added dropwisely to the stirred solution using reflux at ambient temperature. The reaction vessel was placed in an ice bath to decrease the temperature rise of the exothermic reaction. After adding all of FuCl to the DCM solution, the reaction mixture was allowed to stir for an additional 24 h. Purification of FuCl macromers was done by 0.1 N sodium hydroxide (NaOH, Merck Co.). Upon completion of the reaction, the solution was washed several times with water to remove chlorinated propanol products and the solvent was removed by rotovaporation. The macromers were dried in vacuum (0.2 bar) at 30 °C for 24 h and stored at −20 °C until use.

Fourier transform infrared spectroscopy (FTIR, Bruker, Equinox 55, Germany) was perfomed to confirm the presence of the fumarate group in the macromer. FTIR spectra of the PCL-diols and PCLF were collected applying the materials on the KBr disk while it was gently heated up to 35–40 °C and the specimens were examined as KBr disks at room temperature. Differential scanning calorimetry (DSC, NETZSCH (Germany), 200 F3 Maia) measurements were performed in a nitrogen gas atmosphere with the flow rate of 50 mL/min. To keep the same thermal history, each sample was first heated from 25 °C (room temperature) to 80 °C and cooled to −100 °C at a cooling rate of 5 °C/min. Then heating was performed from −100 to 250 °C at a heating rate of 10 °C/min. The glass transition temperature (T_g) was taken as a midpoint of the heat capacity change. The melting point (T_m) and the heat of fusion (ΔH_m) were determined from the maximum endothermic peaks position and integrating of endothermic area. The percent crystallinity (X_c) of PCLF and initial PCL-diol were calculated by using the following equation [23] where ΔH_m^* of pure PCL is 135 J/g.

$$X_c = \left(\frac{\Delta H_m}{\Delta H_m^*}\right) \times 100 \quad (2)$$

2.3. Fabrication of scaffold and coating phase

The replication method includes preparation of green bodies of ceramic foams by coating polymer foam (e.g. polyurethane, PU) with ceramic slurry. The polymer has the desired pore structure with proper internal channel architecture, which can be used as a template for producing ceramic scaffolds. The PU foams cut into a desired shape and size. In order to make the alumina scaffolds, first the ceramic slurry was prepared. The slurry involves alumina powder (Martinswerk, MR70, d50: 0.5–0.8 μm) and water. 0.5% wt% of commercially colloidal silica (Meyco MP320 IR) was added to slurry. Solid content of 75 wt % (43 vol%) was achieved. The polyurethane (PU) template is immersed in the slurry, which subsequently infiltrates the structure and ceramic particles adhere to the surfaces of the polymer. The extra slurry was completely squeezed out by passing the impregnated (PU) sponge through the space of two horizontal steel rollers. The infiltrated sponges were dried at 75 °C for at least 24 h. After drying, the samples were heated at a rate of 1 °C/min to 600 °C. The samples were heated at this temperature for 1 h to burn out the PU foams, and then sintered at a rate of 3 °C/min to 1650 °C for 3 h. The process of polymer burnout was integrated with sintering to avoid handling of the green body.

X-ray diffraction (XRD, D500, Siemens, Germany) was used to detect the phase composition of the scaffold. Also the morphology of scaffold was observed by using scanning electron microscopy (SEM, XL30, Philips, Holland).

The water absorption method based on Archimedes' principle (ASTM C 20-00, 2000), Eq. (3), was used for determining the open porosity of alumina scaffold. The open porosity (P_{open}) is calculated as the ratio of the open pore volume (W–D) to the exterior volume (W–S), where, W, D and S are the saturated weight, dry weight and suspended weight, respectively.

$$P_{open} = \frac{(W-D)}{(W-S)} \times 100 \quad (3)$$

The pore size of alumina scaffold was measured using the SEM micrographs. The average pore size was calculated by measuring the size of 20 pores using the image analysis software [24].

The compression tests of alumina scaffolds were performed using a universal testing machine (Santam, STM-20, Iran) on five samples. The specimens were examined at a crosshead speed of 0.5 mm/min at room temperature. The load and displacement data were recorded in the computer to provide the stress–strain curves to determine the compressive strength. Stress (σ), strain (ε), and Young's modulus (E) were calculated for each ratio in order to evaluate the mechanical strength of each scaffold. Stress was calculated by dividing the force applied by the surface area, while strain was determined by dividing the displacement by the original height of the samples. Stress versus

strain was graphed, and the corresponding Young's modulus was derived from the slope of the graph.

In order to make a chemical link between the alumina scaffolds and the polymer coatings, the silane coupling agent [Methacryloxypropyl trimethoxysilane (MTMS, Silane A174, Merck Co.), $C_{10}H_{20}O_5Si$] was used. Alumina is a bioinert material and does not have any active agents (such as hydroxyl) on its surface [25]. For hydroxylation on the surface of alumina scaffolds, sulfuric acid (H_2SO_4, Merck Co.) was diluted (40% v/v) in distilled water. Then a solution of diluted sulfuric acid and hydrogen peroxide (H_2O_2, Merck Co.) was prepared (the volume ratio of diluted sulfuric acid to hydrogen peroxide = 6). The scaffolds were put in acidic solution at 80 °C for 4 h. Finally, the treated scaffolds were washed in distilled water and ethanol and heat treated at 160 °C for 1 h.

The silanization process was performed on the surface of hydroxylated scaffolds. Samples were sunk in 3 solutions of MTMS (1, 3, 4 g in methanol:distilled water 80:20% v/v) for 2 h at a pH between 3.5 and 4 [26]. A Nicolet 8700 FTIR Spectrometer was used to investigate the structural changes of scaffolds after silanizations. Acetic acid was used as the catalyst for hydrolyzing the silane coupling agents. The samples were rinsed in deionized water and ethanol. After that, they were heat treated in the oven at 160 °C for 1 h. The morphology observation was acquired by the scanning electron microscopy (SEM, XL30, Philips, Holland). The details of the solutions' formulation for silanization are shown in Table 1.

Unsaturated PCLF backbones can be crosslinked more by thermal or photoradical polymerization [27]. HA/PCLF nanocomposites with HA content of 10, 20 and 30 wt% were made. First, 3 g PCLF was dissolved in 100 cm^3 dichloromethane (DCM), 1% (w/w) benzoyl peroxide (BPO, Merck, Co.) and trimethylolpropane trimethacrylate (TMPTMA, Merck, Co.). The reactive diluent (TMPTMA) was used to facilitate crosslinking reactions and also reduce viscosity for better organic phase mixing. The molar ratio of TMPTMA as a crosslinker agent was calculated as much as the double bonds of PCLF in the solution. Then, different amounts of HA nanopowders were mixed with the polymer solution by a magnetic stirrer. After that, the solution was sonicated 3 times by ultrasound energy for 10 min. Ultrasound energy was applied directly to the mixture by an ultrasonic cell disruptor.

The alumina samples were gradually covered with nanodispersion of PCLF/HA by the dipping process. The scaffolds were immersed for 30 min and the coating process was repeated 2 times. The thermal crosslinking process of PCLF macromers was carried out at 70 °C for 30 min to induce the curing reaction and then at 90 °C for 30 min to complete the double bonds conversion. The curing process was repeated after each time dip coating. A Nicolet 8700 FTIR Spectrometer was acquired for investigation of structural evaluation of the coated scaffolds. The morphology of the coated scaffolds was observed by (SEM, XL30, Philips, Holland). The detailed formulations of solutions for coated scaffolds are summarized in Table 1.

3. Result and discussion:

3.1. Characterization of nano-HA powder

X-ray diffraction (XRD) pattern of the powder is given in Fig. 2. The XRD pattern for HA has many peaks in the range from about 7° to about 70° 2θ $Cu_{K\alpha}$. The characteristic peaks are in the range of $2\theta = 25$–$35°$ that was identified according to JCPDS File Cards no. 09-0432. According to the Scherrer Eq. (1) the size of HA crystallites was around 11 nm. The high intensity of the peaks proves that the HA-nanopowder has good crystallinity.

The morphology of nano-HA powder was investigated by SEM and TEM (Fig. 3). SEM image (Fig. 3A) indicates that the powder is consisted of nanoparticles with soft agglomerates in some areas. The TEM image shows that the particles are composed of the nanocrystallites with diameter of 10–100 nm. These images exhibit that nano-HA has a narrow size distribution.

Table 1
Compositions of silanes and nanocomposites solutions.

Sample ID	Solution	MTMS (g)	Dipping time (min)	Heat treatment temp. (°C)	Heat treatment time (min)	Repeating of immersion	PCLF (g)	BPO/ PCLF(wt%)	HA/PCLF (wt%)
S1	Methanol (80 vol%) Distilled water (20 vol%)	1	120	160	60	1	–	–	–
S2	Methanol (80 vol%) Distilled water (20 vol%)	3	120	160	60	1	–	–	–
S3	Methanol (80 vol%) Distilled water (20 vol%)	4	120	160	60	1	–	–	–
C10	DCM (100% vol%)	–	30	Step1:70 °C Step2:90 °C	Step1:30 min Step2:30 min	2	3	1	10
C20	DCM (100% vol%)	–	30	Step1:70 °C Step2:90 °C	Step1:30 min Step2:30 min	2	3	1	20
C30	DCM (100% vol%)		30	Step1:70 °C Step2:90 °C	Step1:30 min Step2:30 min	2	3	1	30

3.2. Characterization of PCLF macromer

FTIR was used to confirm the presence of the fumarate groups in PCLF and the structural changes of PCL-diol to PCLF macromer. FTIR spectra of PCL-diol and PCLF macromer are shown in Fig. 4. The absorption peak for hydroxyl end groups (–OH) of PCL-diol at around 3400 cm^{-1} was reduced which means the molar mass of resulting PCLF macromer is higher than that PCL-diol as the starting material. The weak absorption bands with peak positions at 1260 and 1300 cm^{-1} are due to the C–H rocking vibration of the disubstituted fumarate group and at 1645 cm^{-1} due to C=C stretching, which are absent in the spectrum of PCL [12]. The peaks at 1163 cm^{-1} for PCL-diol and 1156 cm^{-1} for PCLF macromer are related to asymmetric coupled vibrations of C–C(=O)–O and O–C–C groups of PCL. The characteristic ester carbonyl (C=O) stretching band at around 1720 cm^{-1} was detected in both spectra of PCL-diol and PCLF macromer. The stretching, scissoring and asymmetric bending, symmetric bending peaks related to methylene (C–H) are evident at around 2945 cm^{-1}, 1460 cm^{-1} and 1400 cm^{-1}, respectively. These results have proved that PCL-diol was converted successfully to unsaturated PCLF macromer by polycondensation reaction with FuCl.

Thermal properties of PCL-diol and PCLF were investigated by differential scanning calorimetry (DSC) as shown in Fig. 5. DSC was used to measure the glass transition temperature (T_g), melting point (T_m), and heat of fusion (ΔH_m) of the polymer samples. T_g was determined as the midpoint temperatures of the glass transitions. Also, the crystallinity percent (X_c, equation 2) of macromer and its precursor was estimated and the results were summarized in Table 2. PCL is a semicrystalline and

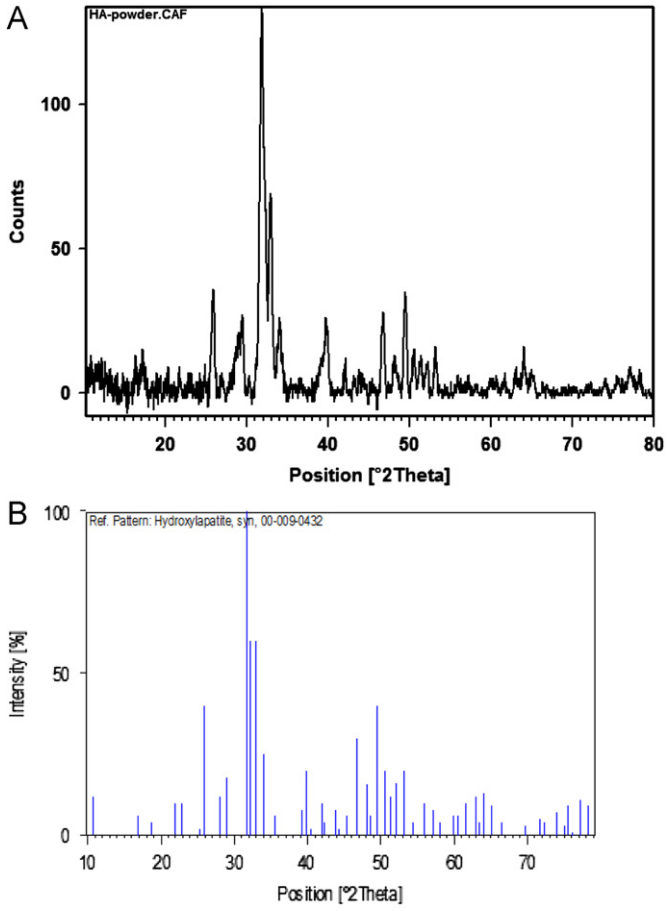

Fig. 2. (A) XRD pattern of nano-HA powder and (B) JCPDS reference lines of hydroxyapatite.

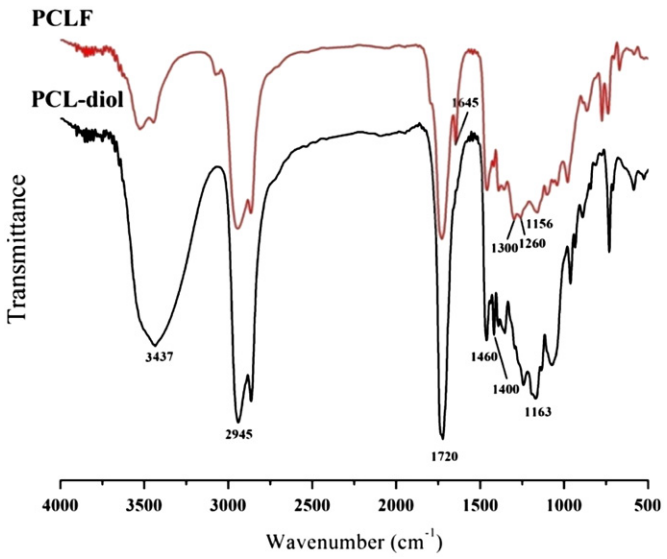

Fig. 4. FTIR spectra of PCL-diol and PCLF macromer.

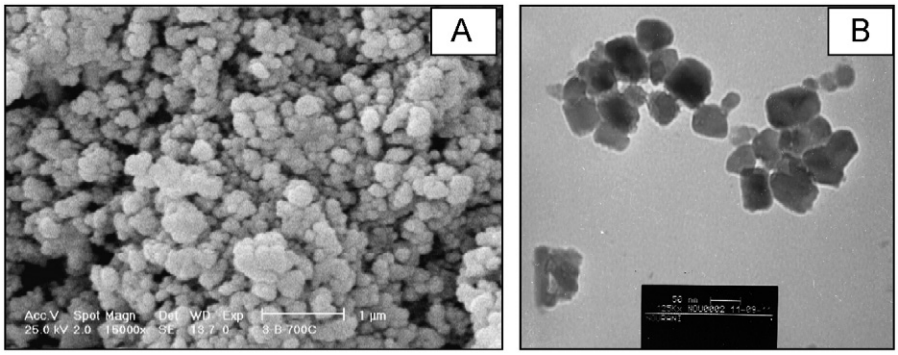

Fig. 3. Morphology study of nanoHA particles; (A) SEM and (B) TEM.

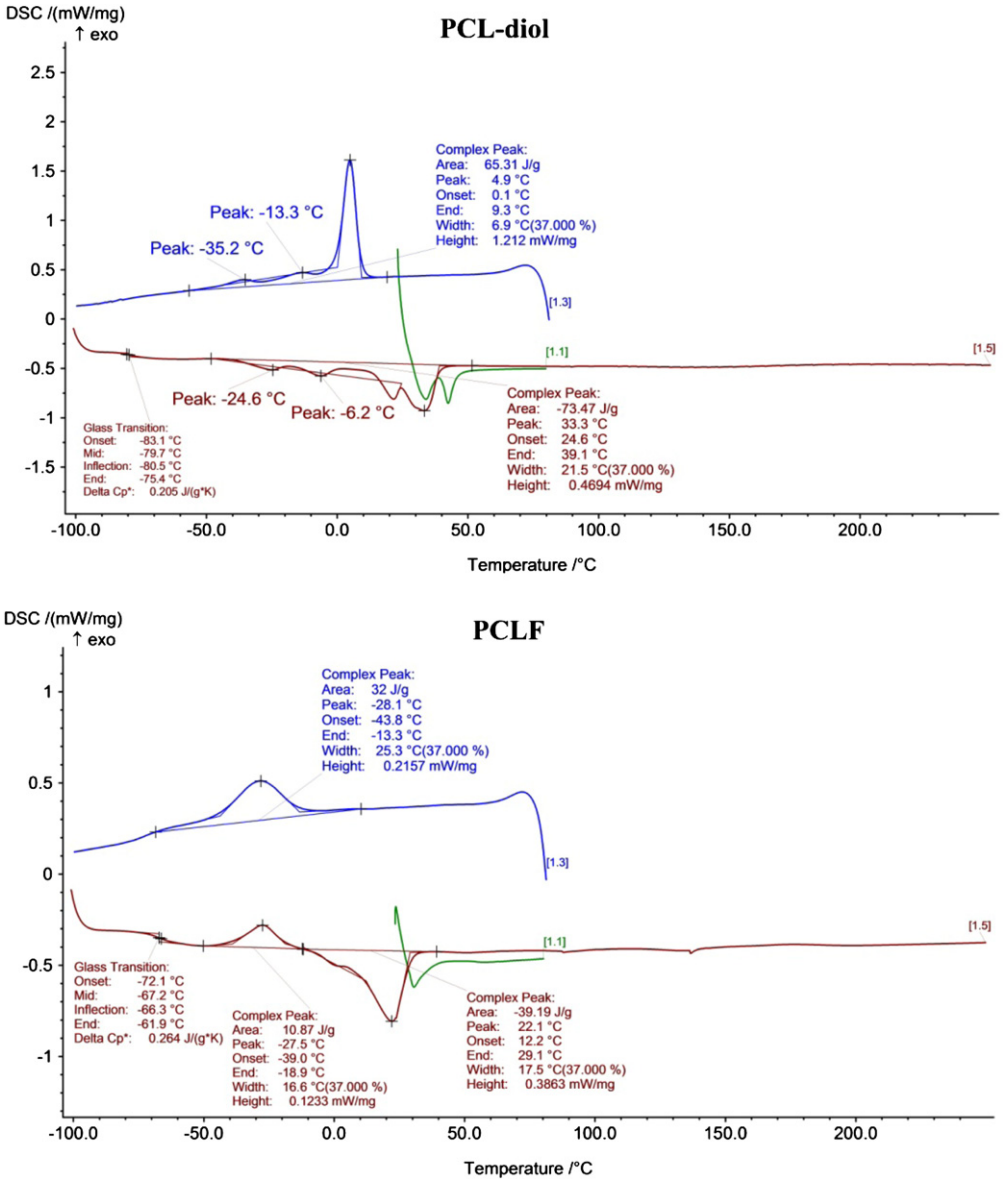

Fig. 5. DSC curves of PCL-diol and PCLF.

Table 2
DSC results of PCL-diol precursors and the synthesized PCLF macromers.

Sample	T_g (°C)	T_m (°C)	Crystallinity (%)	ΔH_m (J g^{-1})
PCL-diol	−79.7	33.3	36	8.98
PCLF	−67.2	21.81	29.02	39.19

linear resorbable aliphatic polyester polymer with a T_m around 30–50 °C and a T_g around −60 °C, depending on the molecular weight [28]. The melting point and the heat of fusion of PCLF is different than that of PCL-diol which can be attributed to the changes in the chains structure. The crystallinity of PCLF decreased from 7% after copolymerization from PCL-diol. The formation of double bonds fumarate groups in the chain of PCLF prevents the crystallization of macromer because of the close packing space.

3.3. Characterization of scaffolds

The alumina scaffolds were processed using a classical foam replication technique. The XRD analysis of the alumina scaffold is shown in Fig. 6. The characteristic

peaks are in the range of $2\theta = 25–60^{\circ}$ that was identified according to JCPDS File Cards no. 00-002-0921. It is evident that all peaks in the samples belong to corundum phase.

The open porosity of the fabricated sample was derived from the density. The porosity of the alumina scaffold, as measured with the Archimedes method in distilled water, was around 82%.

The mechanical properties of alumina scaffolds are summarized in Table 3. The average Young's modulus of alumina scaffolds was 2.8 GPa. The value of Young's modulus of the human cancellous bone reported in the literatures is ranging from 0.05 to 0.5 GPa [1,29]. These results confirmed that the prepared alumina scaffolds have the mechanical strength similar to cancellous bone tissue.

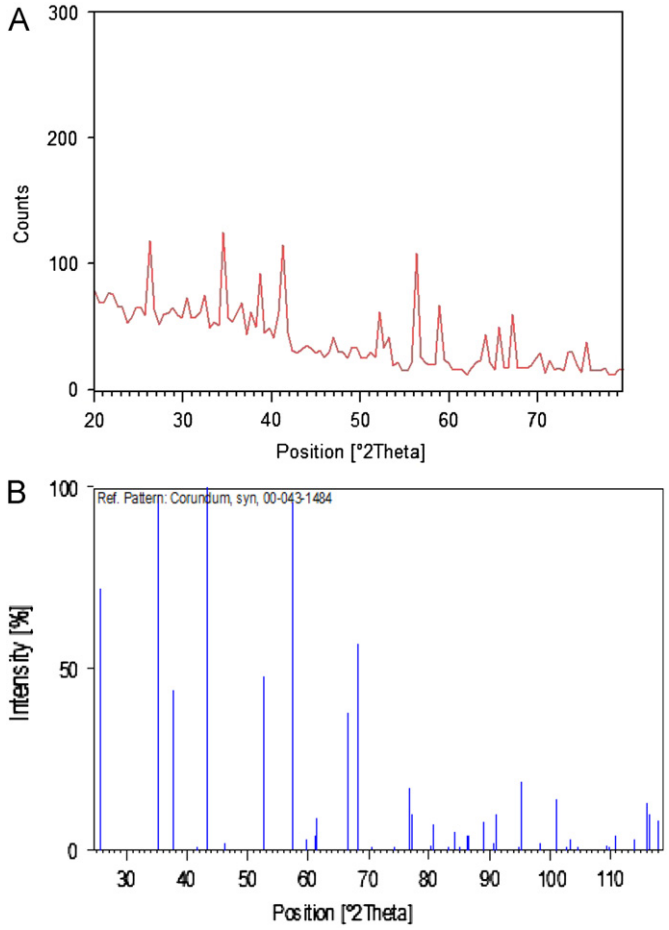

Fig. 6. (A) XRD pattern of alumina scaffold and (B) JCPDS reference lines of corundum.

Table 3
Mechanical properties of the alumina scaffolds.

Sample ID	Force (N)	Stress (MPa)	Elongation (%)	Young's modulus (MPa)
1	162.40	18.04	0.664	2717
2	130.44	14.49	0.507	2859
3	163.34	18.15	0.634	2864
4	185.54	20.62	0.780	2635
5	188.70	20.97	0.754	2871

In order to make a chemical link between alumina scaffolds and polymer coating, MTMS silane coupling agent was used. Alumina is a bioinert material and does not have any active agents (such as hydroxyl) on its surface [25].

The silanization process was performed on the surface of hydroxylated scaffolds. Fig. 7 shows the FTIR spectra of silanized scaffolds. The broad peak around 3400 cm^{-1} is related to stretching vibration mode of water absorption and the peak at 1621 cm^{-1} is related to bending mode of water. As can be seen, the amount of water absorption has enhanced by increasing of silane content. Two stretching peaks corresponding to Si–O–Si and Si–O bonds are observed at wave numbers around 1045 cm^{-1} and 1112 cm^{-1}. Also, the peak around 1457 cm^{-1} is related to CH_3–R bond [30].

Because the CH_2 content in the silanized scaffolds is approximately proportional to the peak area ratio of CH_2 ($\approx$2820–3075 cm^{-1}) bond to that of Al–O ($\approx$500–650 cm^{-1}) bond, the peak area ratio of the CH_2 to Al–O has been used for determining the CH_2/Al–O (%) value in the films after silanization. All FTIR spectra were normalized and the areas related to CH_2 and Al–O bonds were estimated by the Thermo Nicolet OMNIC® 6.1a software and results were summarized in Table 4.

The CH_2 amount and the area ratio of CH_2/Al–O bonds were decreased by enhancing of silane content. This means the minimum amount of silane (sample S1) is sufficient as a thin interface layer between scaffold and polymer.

Fig. 8 shows the FTIR spectra of PCLF/nano-HA coatings on alumina scaffolds. The peak at around 1645 cm^{-1} is related to stretching vibration mode and the large peak at around 3422 cm^{-1} corresponds to stretching vibration of water absorption. The P–O bands ($\sim$500–600 and 900–1200 cm^{-1}, characterize the typical apatite structure. The sharpness of these peaks was enhanced by HA in the coatings. The peak at around 3739 cm^{-1} is contributed to O–H vibration.

The weak absorption bands at 1645 cm^{-1} are due to C=C stretching of PCLF [11]. The characteristic ester carbonyl (C=O) stretching band at around 1736 cm^{-1} was detected in all samples. The asymmetric stretching, symmetric stretching, scissoring and stretching modes of methylene (C–H) are evident at around 2928 cm^{-1}, 2830 cm^{-1}, 1460 cm^{-1} and 3850 cm^{-1}, respectively.

Fig. 9 shows the SEM images of alumina scaffolds before and after coating by PCLF/nano-HA composite layer. It is visible that the scaffolds were constituted of interconnected and homogeneously distributed pores with the average sizes ranging 200–900 μm. The macroscopic pores network in the scaffold is a necessary tool to promote cell seeding distribution, cell migration throughout the 3D space, exchange of waste products and neovascularisation after in vivo implantation of the scaffold [31]. Pore size of scaffolds for bone regeneration should be bigger than 100 μm, and the pores should be

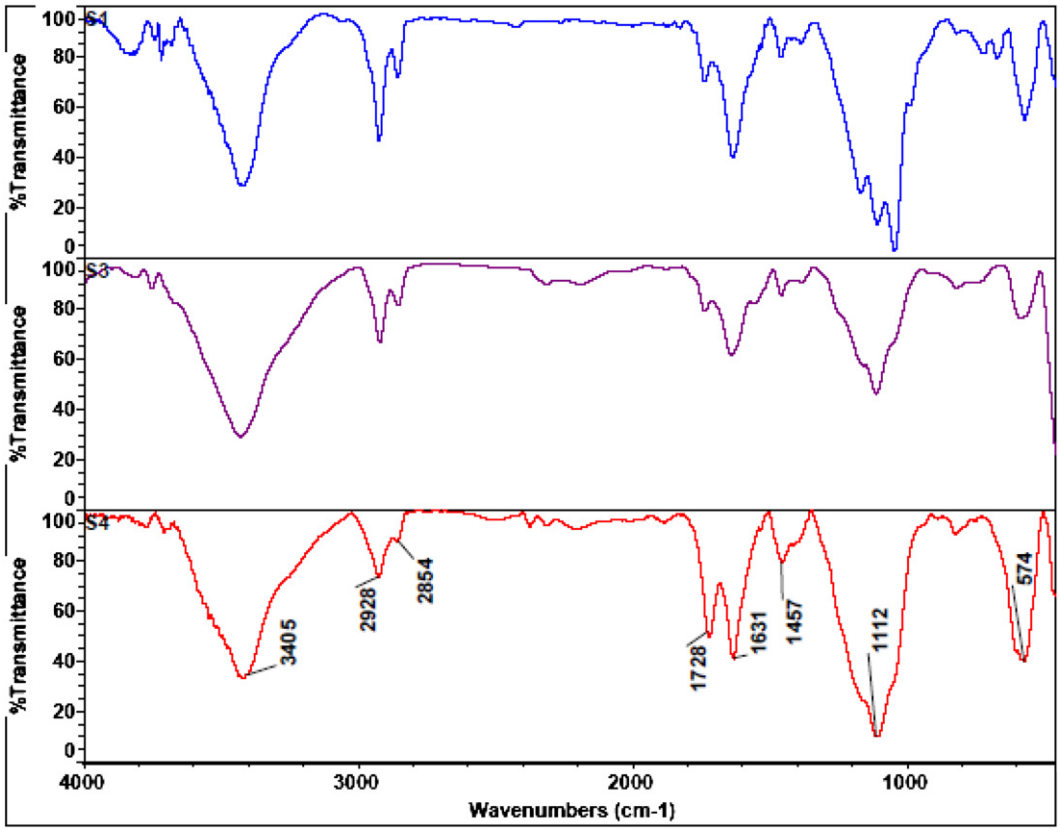

Fig. 7. FTIR spectra of alumina scaffolds after silanization.

Table 4
Comparison of the FTIR area peaks related to CH_2 and Al–O bonds.

Sample (ID)	Wave number related to CH_2 bond	Area peak related to CH_2 bond	Wave number related to Al–O bond	Area peak related to Al–O bond	Area ratio of CH_2/Al–O bonds
S_1	2821–3057	3923.48	506–636	2551.79	1.54
S_3	2814–2994	2324.62	512–642	1526.41	1.52
S_4	2824–3024	2381.39	506–712	6082.57	0.39

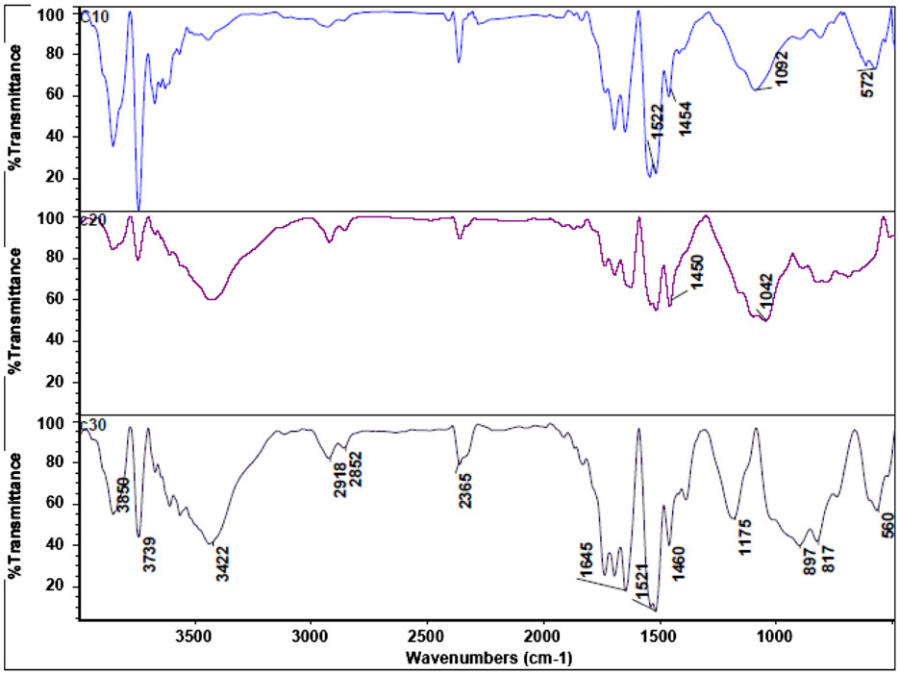

Fig. 8. FTIR spectra of PLCF/nano-HA composites on alumina scaffold.

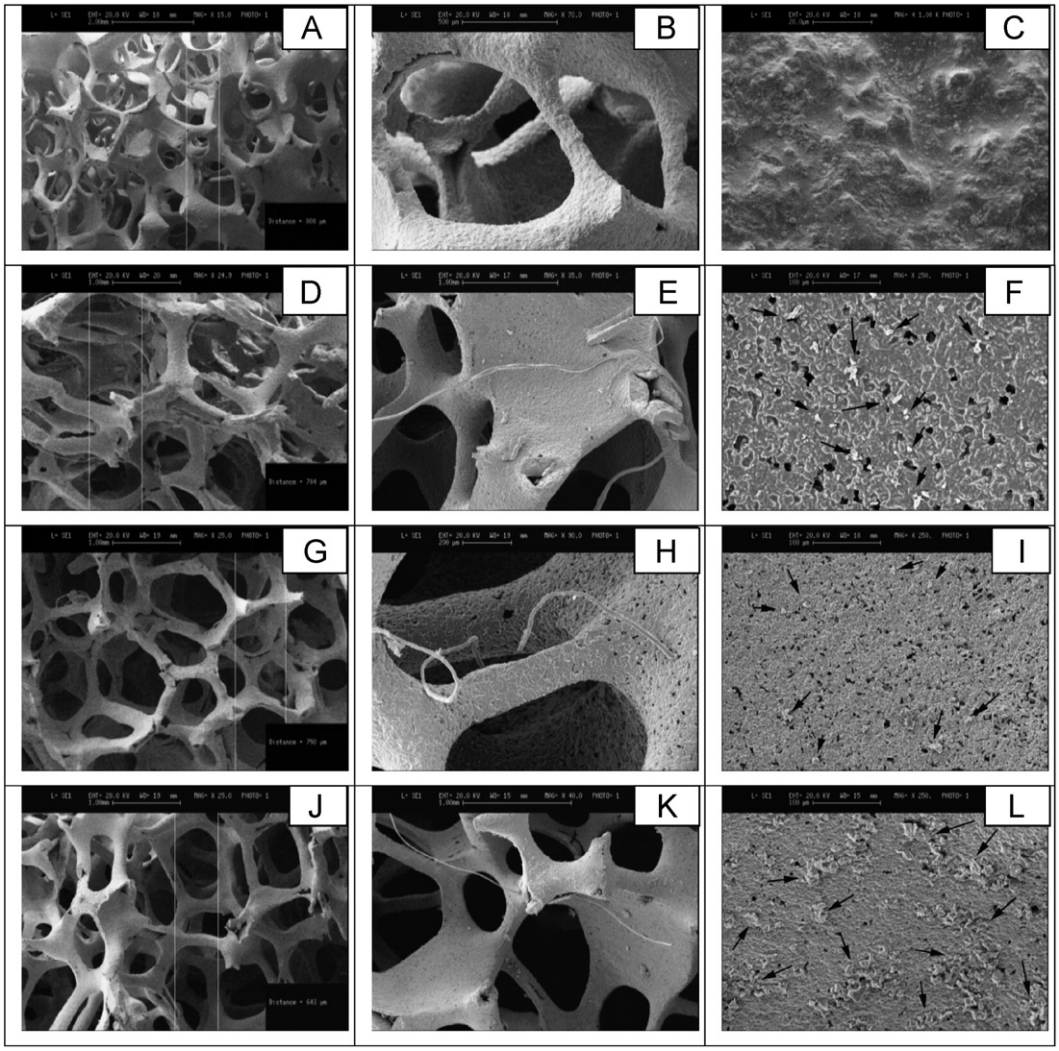

Fig. 9. SEM images of alumina scaffolds (A–C) before and (D–L) after coating with nano-HA/PCLF; (D–F) sample C10, (G–I) sample C20, (J–L) sample C30. The arrows indicate the HA particle distributions on the surfaces of coatings.

interconnected [31]. This parameter can be thoroughly characterized by SEM images, which means the scaffolds of this research are good candidates for future *in vitro* and *in vivo* studies.

Fig. 9(E, H, K) shows the PCLF filaments beside HA nanoparticles (the particles have been shown by arrows). As can be seen in Fig. 9(F, I, L), the HA nanoparticles formed agglomerates in some areas. Agglomeration was enhanced by increasing of nanoHA percent in the coating solutions. Hydroxyapatite promotes the bone regeneration in human body [32]. Nano porosities are visible on the surfaces of coated samples which decreased in the sample C30. These porosities are essential for the molecule transport crucial for signaling, any cell nutrition and waste removal [33]. The formation of the small porosities on the surface of alumina can be related to soaking of the scaffolds in the sulfuric acid/hydrogen peroxide solution before silanization stage. These nanocomposite layers can be a good carrier for drugs and other biomolecules and bioactive agents for future studies.

4. Conclusion

In the present study PCLF/nano-HA coatings were performed on alumina scaffolds. Nano-HA powder was synthesized successfully by the sol–gel method. The presence of nano-HA in poly(ε-caprolactone fumarate) (PCLF) as a carrier on the surface of alumina scaffold was performed. MTMS silane coupling agent was used for making a chemical link between the alumina scaffolds and the polymer coating. The results of this investigation show that using of 1 g MTMS in 100 g solvent is sufficient for making a thin interface layer between scaffold and polymer. The coated scaffolds were constituted of interconnected and homogeneously distributed macropores. The alumina scaffolds showed appropriate mechanical properties with high porosity. HA distribution and agglomerates on surface of scaffolds were enhanced by increasing of nanoHA percent in the coating solutions. This research will serve as a base for future studies related to *in vitro* and *in vivo* tests to find a good candidate for bone tissue regeneration.

References

[1] L.L. Hench, J. Wilson, Introduction, in: 1st ed., in: L.L. Hench, J. Wilson (Eds.), An Introduction to Bioceramics, 1, World Scientific Publishing, Singapore, 1993, pp. 1–24.

[2] L.L. Hench, Bioceramics: from concept to clinic, Journal of the American Ceramic Society 74 (7) (1991) 1487–1510.

[3] N. Tamai, A. Myoui, T. Tomita, T. Nakase, J. Tanaka, T. Ochi, H. Yoshikawa, Journal of Biomedical Materials Research 59 (1) (2002) 110–117.

[4] K.A. Hing, International Journal of Applied Ceramic Technology 2 (3) (2005) 184–199.

[5] S.J. Hollister, Porous scaffold design for tissue engineering, Nature Materials 4 (2005) 518–524.

[6] K. Rezwan, Q.Z. Chen, J.J. Blaker, A.R. Boccaccini, Biodegradable and bioactive porous polymer/metallic composite scaffolds for bone tissue engineering, Biomaterials 27 (2006) 3413–3431.

[7] A. Guidara, K. Chaari, J. Bouaziz, Elaboration and characterization of alumina fluorapatite composites, Journal of Biomaterials and Nanobiotechnology 2 (2011) 103–113.

[8] X. Wang, R.A. Bank, J.M. Tekoppele, C.M. Agrawal, The role of collagen in determining bone mechanical properties, Journal of Orthopaedic Research 19 (2001) 1021–1026.

[9] S. He, M.J. Yaszemski, A.W. Yasko, P.S. Engel, A.G. Mikos, Injectable biodegradable polymer composites based on poly(propylene fumarate) crosslinked with poly(ethylene glycol)-dimethacrylate, Biomaterials 21 (2000) 2389–2394.

[10] D. Hakimimehr, D.M. Liu, T. Troczynski, In-situ preparation of poly(propylene fumarate)–hydroxyapatite composite, Biomaterials 26 (2005) 7297–7303.

[11] K.S. Brink, P.J. Yang, J.S. Temenoff, Degradative properties and cytocompatibility of a mixed-mode hydrogel containing oligo[poly(ethylene glycol)fumarate] and poly(ethylene glycol)dithiol, Acta Biomaterialia 5 (2009) 570–579.

[12] E. Jabbari, S.F Wang, L.C. Lu, J.A. Gruetzmacher, S. Ameenuddin, T.E. Hefferan, B.L. Currier, A.J. Windebank, M.J. Yaszemski, In vitro migration and proliferation of human osteoblasts in injectable in situ crosslinkable poly(caprolactone fumarate) scaffolds, Biomacromolecules 6 (2005) 2503–2511.

[13] S. Sharifi, H. Mirzadeh, M. Imani, M. Atai, F. Ziaee, Photopolymerization and shrinkage kinetics of in situ crosslinkable N-vinyl-pyrrolidone/poly(epsilon-caprolactone fumarate) networks, Journal of Biomedical Materials Research (A) 84 (2008) 545–556.

[14] S. Sharifi, H. Mirzadeh, M. Imani, F. Ziaee, M. Tajabadi, A. Jamshidi, M. Atai, Synthesis, photocrosslinking characteristics, and biocompatibility evaluation of N-vinyl pyrrolidone/polycaprolactone fumarate biomaterials using a new proton scavenger, Polymers for Advanced Technologies 19 (2008) 1828–1838.

[15] S. Sharifi, M. Kamali, N.K. Mohtaram, M.A. Shokrgozar, S.M. Rabiee, M. Atai, M. Imani, H. Mirzadeh, Preparation, mechanical properties, and in vitro biocompatibility of novel nanocomposites based on polyhexamethylene carbonate fumarate and nanohydroxyapatite, Polymers for Advanced Technologies 29 (2009) 605–611.

[16] Y. Shafieyan, S. Sharifi, M. Imani, M.A. Shokrgozar, N. Aboudzadeh, M. Atai, A biocompatible composite based on poly(e-caprolactone fumarate) and hydroxyapatite, Polymers for Advanced Technologies 22 (2011) 2182–2190.

[17] S.I. Roohani-Esfahani, S. Nouri-Khorasani, Z. Lu, R. Appleyard, H. Zreiqat, The influence hydroxyapatite nanoparticle shape and size on the properties of biphasic calcium phosphate scaffolds coated with hydroxyapatite–PCL composites, Biomaterials 31 (2010) 5498–5509.

[18] G.L. Witucki, A. Silane Primer, Chemistry and applications of alkoxy silanes, Journal of Coatings Technology 65 (822) (1993) 57–60.

[19] K. Schwartzalder, A.V. Somers, Method of making a porous shape of sintered refractory ceramic articles, United States Patent no. 3090094, 1963.

[20] S.C. Cowin (Ed.), Bone Mechanics, CTC Press, Boca Raton, FL, 1989, pp. 1–4 10-1–10-23.

[21] L.J. Gibson, M.F. Ashby, Cellular Solids: Structure and Properties, 2nd ed., Pergamon, Oxford, 1999, pp. 429–452.

[22] B.D. Cullity, Elements of X-ray diffraction, in: Morris Cohen (Ed.), Addison-Wesley publishing, San Diego, 1977.

[23] Y.M. Lim, H.J. Gwon, J.H. Choi, J. Shin, Y.C. Nho, Preparation and biocompatibility study of gelatin/kappa-carrageenan scaffolds, Macromolecular Research 18 (2010) 29–34.

[24] J. Brandrup, E.H. Immergut (Eds.), 3rd ed., Wiley, New York, 1989.

[25] H. Fischer, C. Niedhart, Bioactivation of inert alumina ceramics by hydroxylation, Biomaterials 26 (2005) 6151–6157.

[26] Y.C. Yang, S.B. Jeong, B.G. Kim, P.R. Yoon, Examination of dispersive properties of alumina treated with silane coupling agents, by using inverse gas chromatography, Powder Technology 191 (1–2) (2009) 117–121.

[27] S. Sharifi, H. Mirzadeh, M. Imani, Z. Rong, A. Jamshidi, M.A. Shokrgozar, M. Atai, N. Roohpour, Injectable in situ forming drug delivery system based on poly(epsilon-caprolactone fumarate) for tamoxifen citrate delivery: gelation characteristics, in vitro drug release and anti-cancer evaluation, Acta Biomaterialia 5 (2009) 1966–1978.

[28] I. Engelberg, J. Kohn, Physico-mechanical properties of degradable polymers used in medical applications: a comparative study, Biomaterials 12 (1991) 292–304.

[29] K. Rezwan, Q.Z. Chen, J.J. Blaker, A.R. Boccaccini, Biodegradable and bioactive porous polymer/inorganic composite scaffolds for bone tissue engineering, Biomaterials 27 (2006) 3413–3431.

[30] Z. Li, W.T. Jiang, H. Hong, An FTIR investigation of hexadecyltrimethylammonium intercalation into rectorite, Spectrochimica Acta Part A: Molecular and Biomolecular Spectroscopy 71 (2008) 1525–1534.

[31] M. Zilberman, Active Implants and Scaffolds for Tissue Regeneration, Springer, Heidelberg, 2011, p. 275.

[32] C. Mangano, E.G. Bartolucci, C. Mazzocco, A new porous hydroxyapatite for promotion of bone regeneration in maxillary sinus augmentation: clinical and histologic study in humans, International Journal of Oral and Maxillofacial Implants 18 (2003) 23–30.

[33] B. Müller, H. Deyhle, F.C. Fierz, S.H. Irsen, J.Y. Yoon, S. Mushkolaj, O. Boss, E. Vorndran, U. Gbureck, Ö. Degistirici, M. Thie, B. Leukers, F. Beckmann, F. Wittei, Bio-mimetic hollow scaffolds for long bone replacement, in: Biomimetics and Bioinspiration, (Eds.) Raúl J. Martín-Palma, Akhlesh Lakhtakia, in: Proceeding of SPIE, vol. 7401, 74010D, 2009.